Talanta 102 (2012) 156–163

Contents lists available at SciVerse ScienceDirect

Talanta

journal homepage: www.elsevier.com/locate/talanta

Label-free aptasensor for thrombin determination based on the nanostructured phenazine mediator

Gennady A. Evtugyn [a,*], Veronika B. Kostyleva [a,b], Anna V. Porfireva [a], Maria A. Savelieva [a], Vladimir G. Evtugyn [c], Rusal R. Sitdikov [d], Ivan I. Stoikov [d], Igor S. Antipin [d], Tibor Hianik [b]

[a] Analytical Chemistry Department of Kazan Federal University, 18 Kremlevskaya Street, Kazan 420008, Russian Federation
[b] Department of Nuclear Physics and Biophysics, Comenius University, Mlynska dolina F1, 842 48 Bratislava, Slovakia
[c] Electron Microscopy Laboratory of Biology Faculty of Kazan Federal University, 18 Kremlevskaya Street, Kazan 420008, Russian Federation
[d] Organic Chemistry Department of Kazan Federal University, 18 Kremlevskaya Street, Kazan 420008, Russian Federation

ARTICLE INFO

Available online 8 July 2012

Keywords:
Aptasensor
Thrombin
DNA aptamer
Thiacalixarene
Neutral Red

ABSTRACT

New aptasensors based on DNA aptamer and polycarboxylated thiacalix[4]arenes in *cone*, 1,3-*alternate* and *partial cone* configurations bearing Neutral Red (NR) at substituents at the lower rim have been developed and applied for thrombin detection. The assembly of the biorecognition layer was optimized by AFM and EIS study to reach the maximal coverage and regular composition of the surface layer. The interaction of the NR groups with thrombin suppressed the electron hopping between oxidized and reduced mediator groups. This regularly decreased the NR peak current and increased the resistance of the charge transfer. The aptasensor makes it possible to detect from 1 nM to 1 μM of thrombin with the detection limit of 0.05–0.5 nM. No effect of the 1000 excess of bovine serum albumin on the signal was observed. The influence of thiacalix[4]arene configuration on the sensitivity of aptasensor signal toward thrombin is discussed.

1. Introduction

DNA and RNA aptamers are synthetic oligonucleotides binding low-molecular compounds, proteins and other biomolecules with high specificity and efficiency compared to those of antigen–antibody interactions [1]. The interest toward aptamers expressed in the past decades is related both to the relatively simple strategy of their selection based on a combinatorial chemistry approach and the high potential of their use in the assembly of biorecognition devices, i.e., biosensors, logic gates, electrophoresis, affine chromatography systems, etc. [2]. In comparison with antibodies, the aptamers exhibit long-term stability, a simpler operation mode and a better reproducibility of binding abilities during production and purification. The modification of the aptamers with optical or redox active labels or with functional groups required for immobilization is usually easier than that of antibodies as well [3]. The range of the affinity constant of aptamers toward their substrates varies from micro- to nanomolar values. This offers new opportunities for the highly sensitive detection of various species based on their binding with aptamers in the assembly of appropriate biosensors.

Various strategies are employed for the generation of the biosensor signal related to the aptamer—analyte interaction. Most often, the following approaches are applied: (1) the use of redox labels, i.e., ferrocenes [4–6] , phenothiazine dyes [7–10], thionine [11] which shifts their potential or oxidation current due to a recognition event; (2) conformational changes of the aptamer structure caused by the analyte binding [12–14] and (3) accumulation of the redox labels within the surface layer similar to that of sandwich immunoassay [15–18]. The use of redox labels provides the high sensitivity of the signal measurement. Nevertheless, the further enhancement of the aptasensor assembly is required to simplify the measurement protocol, reduce its cost and labor content.

Nanosized supports for aptamers and redox labels are of special interest in this area. The application of colloidal gold [11,15,17–21] or, carbon nanotubes, [9,22–24] not only amplifies the signal due to electron mediation but also increases the surface loading and accessibility of the aptamer binding sites for the analytes. This results in a faster electron exchange and a lower working potential as well as in a lesser interference with electroactive matrix components.

Thrombin is a multifunctional serine protease that plays an important role in the procoagulant and anticoagulant functions [24,25]. Thrombin is also involved in the other activities like inflammation and wound healing. The first DNA aptamer selective

* Corresponding author.
E-mail address: Gennady.Evtugyn@ksu.ru (G.A. Evtugyn).

0039-9140/$ - see front matter © 2012 Elsevier B.V. All rights reserved.
http://dx.doi.org/10.1016/j.talanta.2012.07.007

to the fibrinogen binding site of thrombin was developed by Bock et al. [25]. It is comprised of the 15-mer sequence 5′-GGT TGG TGT GGT TGG-3′. Later on, Tasset et al. [26] have developed the 29-mer DNA aptamer specific for the heparin binding site of thrombin. The binding motif of both DNA aptamers is formed by G-quartet structure [27], but the binding sites differ from each other. This leads to their different binding affinities toward the target protein. The concentration of thrombin in blood during the coagulation varies from several nanomolar to low micromolar levels [28]. Recently, intraoperative monitoring of thrombin generation in blood showed an increase in its concentration from sub-picomolar to nanomolar levels during surgery [29]. This confirms the importance of the thrombin level monitoring in clinical analysis. The biosensors based on aptamers specific for thrombin provide the sensitivity of its detection required by medical applications and clarify details of various detection protocols which can be promising for other biorecognition phenomena as well.

We have recently shown that the use of nanosized supports for aptamer immobilization and implementation of the mediator on the surface layer offers some advantages over traditional measurement protocols, e.g. a faster response, a higher sensitivity toward thrombin and a lower non-specific sorption for the interferences. Particularly, electropolymerized phenothiazines [8,30,31] and carbon nanotubes [9,32] have been successfully applied for non-covalent electrostatic immobilization of the aptamer and the sensitive detection of thrombin by the QCM and EIS techniques. A phenoxazine dye and Neutral Red (NR), was covalently attached to the terminal carboxylic groups of the substituents at the thiacalix[4]arene core [33] and then used for the voltammetric detection of thrombin based on an appropriate aptamer co-immobilized with a mediator at the glassy carbon electrode (GCE). The thrombin binding suppressed the electron exchange within the surface layer and hence diminished the reduction current related to the mediator redox conversion. The biosensor developed showed a low limit of detection (LOD) of 0.05 nM with an insignificant influence of bovine serum albumin (BSA).

In this work, the label free detection of thrombin was performed based on the above measurement protocol with various configurations of the macrocyclic core and the surface layer was optimized by the EIS and AFM techniques to improve the analytical and operational characteristics of thrombin determination.

2. Experimental

2.1. Reagents

The thiacalix[4]arenes used for mediator modification (Fig. 1) were synthesized at the Organic Chemistry Department of Kazan Federal University as described elsewhere [34].

The structure of thiacalix[4]arene was confirmed by IR, ^{1}H NMR spectroscopy and elemental analysis. The DNA aptamer 5′-GGT TGG TGT GGT TGG TTT TTT TTT TTT TTT 3′-NH_2 specific for thrombin was purchased from Thermo Fisher Scientific GmbH (Ulm, Germany). Human α-thrombin, BSA, NR, 4-(2-hydroxyethyl)-1-piperazineethanesulfonic acid (HEPES), 2-(*N*-morpholino)ethanesulfonic acid (MES), *N*-(3-dimethylaminopropyl)-*N*′-ethylcarbodiimide (EDC) and *N*-hydroxysuccinimide (NHS) were from Sigma-Aldrich (Germany). All the reagents were of analytical grade and used without additional purification. Millipore water was used for the preparation of working solutions.

2.2. Apparatus

Electrochemical measurements were performed with an AUTOLAB PGSTAT 302N potentiostat with an FRA module for EIS measurements (Metrohm Autolab b.v., The Netherlands). A three-electrode cell with working glassy carbon electrode (GCE, 2.5 mm rod inserted into a polytetrafluoroethylene bar, working area 1.67 mm^2, "Graphite", Moscow, Russian Federation), a Pt auxiliary electrode and a double junction Ag/AgCl reference electrode (AUTOLAB cat. no. 6.0726.100) were used in all the electrochemical measurements. EIS parameters were calculated using the NOVA software. AFM measurements were carried out using the scanning probe microscope MultiMode V (Veeco) in the tapping mode in air at ambient temperature with a $5 \times 5\ \mu m^2$ scanner and standard silicon cantilevers. Highly ordered pyrolytic graphite (HOPG), grade ZYH of $15 \times 15 \times 2\ mm^3$ from Advanced Ceramics Co. (Canada) was used in the AFM study as a substrate. Prior to use, the HOPG was cleaved with adhesive tape and imaged to establish its cleanliness.

2.3. Aptasensor preparation

Prior to use, GCE was polished to a mirror-like surface and cleaned with 1.0 M sulfuric acid, NaOH and acetone. Then cyclic

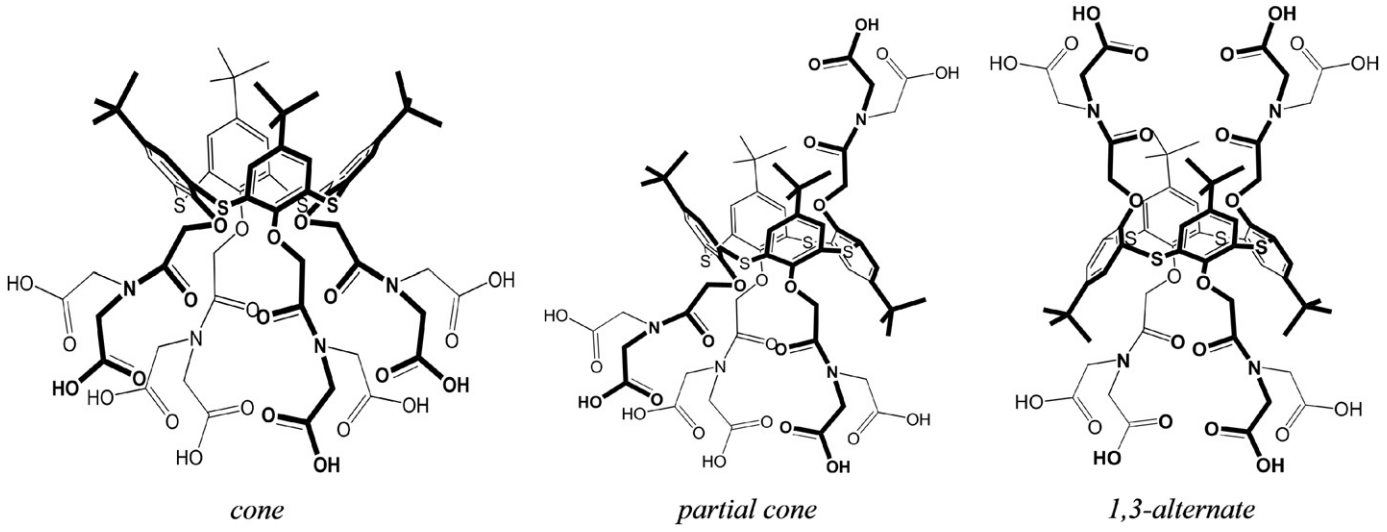

Fig. 1. Configurations of polycarboxylated tetrasubstituted thiacalix[4]arene used for the NR covalent binding.

voltammogram was recorded in the potential range from 0.1 to −1.3 V vs. Ag/AgCl with the scan rate of 0.1 V/s to check the possible influence of electroactive impurities. The electrode was dried and fixed upside down. 2 μL of 1.0 mM of a thiacalix[4]arene solution in glacial acetic acid was placed onto the working surface and dried at ambient temperature (20 °C) for 20 min. After that, 5 μL of 15 mM EDC and 5 μL of 8.7 mM NHS in 0.05 M MES buffer (pH=5.5) were mixed together and immediately dropped onto the thiacalix[4]arene film. The electrode was covered with a plastic tube for 30 min to avoid drying and then washed twice with millipore water and finally with a 0.05 M HEPES buffer (pH=7.0). Then 10 μL of 10 mg/mL NR solution in 0.05 M HEPES was placed onto the electrode. After 15 min, the electrode was washed again and treated with 5 μL of the 0.5 μM aptamer solution in 0.05 mM HEPES (pH=7.0) in a similar manner. The electrode was incubated for 20 min and then washed with millipore water and HEPES buffer solution as described above. The efficiency of NR covalent binding was checked by recording cyclic voltammogram in HEPES buffer solution. The concentrations of NR and aptamer were specified elsewhere [33] to provide their simultaneous binding to carboxylic groups of the thiacalixarene carrier. The aptasensor was stored in a 0.05 M HEPES buffer between measurements.

2.4. Detection of thrombin

The operability of the aptasensor was checked prior to thrombin determination by voltammetric measurement of the NR characteristics (peak current and potential) and impedimetric estimation of the charge transfer resistance and capacity. Then the aptasensor was rinsed with a HEPES buffer and fixed upside down. 10 μL of a thrombin solution was spread onto the working surface. After 10 min of incubation, the aptasensor was rinsed with water and placed in the working cell with 5 mL of 0.05 M HEPES containing 0.1 mM $K_3[Fe(CN)_6]$. The voltammogram was recorded after 3 min equalization in the conditions mentioned for the NR modified electrode (Section 2.3). The shift of the reduction peak current due to the contact of the aptasensor with thrombin was calculated as an aptasensor signal.

Each biosensor can be used for at least 10 measurements. The regeneration of the aptasensor is reached similarly to that described in [35] by treating with 1.0 M NaCl for 30 min. Also, the consecutive addition of separate samples of thrombin solutions is possible with summation of their signals confirmed by comparison of the signals with the results of one-step addition of the same thrombin concentration. In order to take into account the variation of the surface layer in the manufacture, all the electrochemical measurements were performed in six repetitions with the intermediate renewal of the biorecognition layer.

The EIS measurements were performed in the presence of an equimolar mixture of 0.01 M $K_3[Fe(CN)_6]$ and 0.01 M $K_4[Fe(CN)_6]$ at the potential (+0.235 V) calculated as a half-sum of the peak potentials of the redox couple $[Fe(CN)_6]^{3-/4-}$. The amplitude of the applied sine potential was 5 mV. The EIS spectra were recorded within the frequency from 100 kHz to 0.04 Hz with a sampling rate of 12 points per decade. The calculations of capacitance and the charge transfer resistance from EIS spectra were made using fitting procedure corresponding to the equivalent circuit shown in Scheme 1. Here R_S and R_{et} are electrolyte and electron transfer resistances, respectively, Z_W is the Warburg impedance and C is the capacitance of the electrode surface/solution interface. The R_{et} and C values reflect the changes in the charge distribution and diffusional permeability of the surface layer due to aptamer–thrombin interactions whereas the R_S was quite constant.

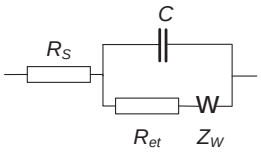

Scheme 1

3. Results and discussion

3.1. AFM investigation of the surface coating

The coverage of the transducer surface with a thiacalix[4]arene layer and the morphology of its surface were investigated using AFM on the HOPG. The *partial cone* (*paco*) configuration was taken as an example. Various amounts of thiacalix[4]arenes were spread along the surface, dried and then topographical images were obtained to establish the size and distribution of the particles (Fig. 2). Taken in the concentration less than 5 nM/cm^2, the thiacalix[4]arenes form tuberous incomplete films with numerous raptures. A significant part of the HOPG surface remains uncovered. The particles with the average size of about 50 nm and a height of 6–8 nm are uniformly distributed along the electrode surface (Fig. 2A, B). Probably they correspond to the supramolecular aggregates of thiacalix[4]arene stabilized by intermolecular hydrogen bonds of carboxylic groups [36]. An increase of the macrocycle content to 50 nM/cm^2, nearly to that used in the aptasensor assembly, resulted in the formation of a dense film about 4 nm thick. The average size of the aggregates increased to 150–180 nm while their height diminished to 4–6 nm (Fig. 2C, D).

The same samples of the HOPG covered with thiacalix[4]arene were consecutively treated with an EDC–NHS mixture and an excessive amount of the NR was added in order to covalently attach them onto the calixarene surface similar to the procedure used for the electrochemical aptasensor preparation (see Section 2.3). The NR attachment significantly increased the roughness of the surface and decreased the uniformity of the particle distribution. Instead of rather small holes comparable with the particles, there appeared large cavities of naked HOPG (Fig. 2E for low thiacalix[4]arene loading). Increase in the thiacalix[4]arene surface concentration made it possible to fully cover the support surface after the NR attachment (Fig. 2F). Nevertheless, the size of the particles remained about the same (150–250 nm) although their size along the average interface increased to 35–40 nm. The comparison of the reproducibility of the surface morphology was also much better for higher quantities of the macrocycle.

To reach a full coverage of the surface and a regular distribution of the relief elements, the electrochemical experiments have been therefore performed with the surface concentration of the thiacalixarenes of about 50 nM/cm^2.

3.2. Voltammetric measurements

As shown earlier for the *paco* isomer of the polycarboxylated thiacalix[4]arene [33], the carbodiimide binding provides the covalent NR attachment to the terminal carboxylic groups of the substituents as it is demonstrated in Scheme 2.

In all the experiments, an excessive amount of the NR over that corresponding to the number of carboxylic groups in the macrocyclic carrier was taken. The reaction period (30 min) was chosen to reach a stable reproducible response related to the maximal amount of substituted terminal groups. The voltammograms obtained (Fig. 3)

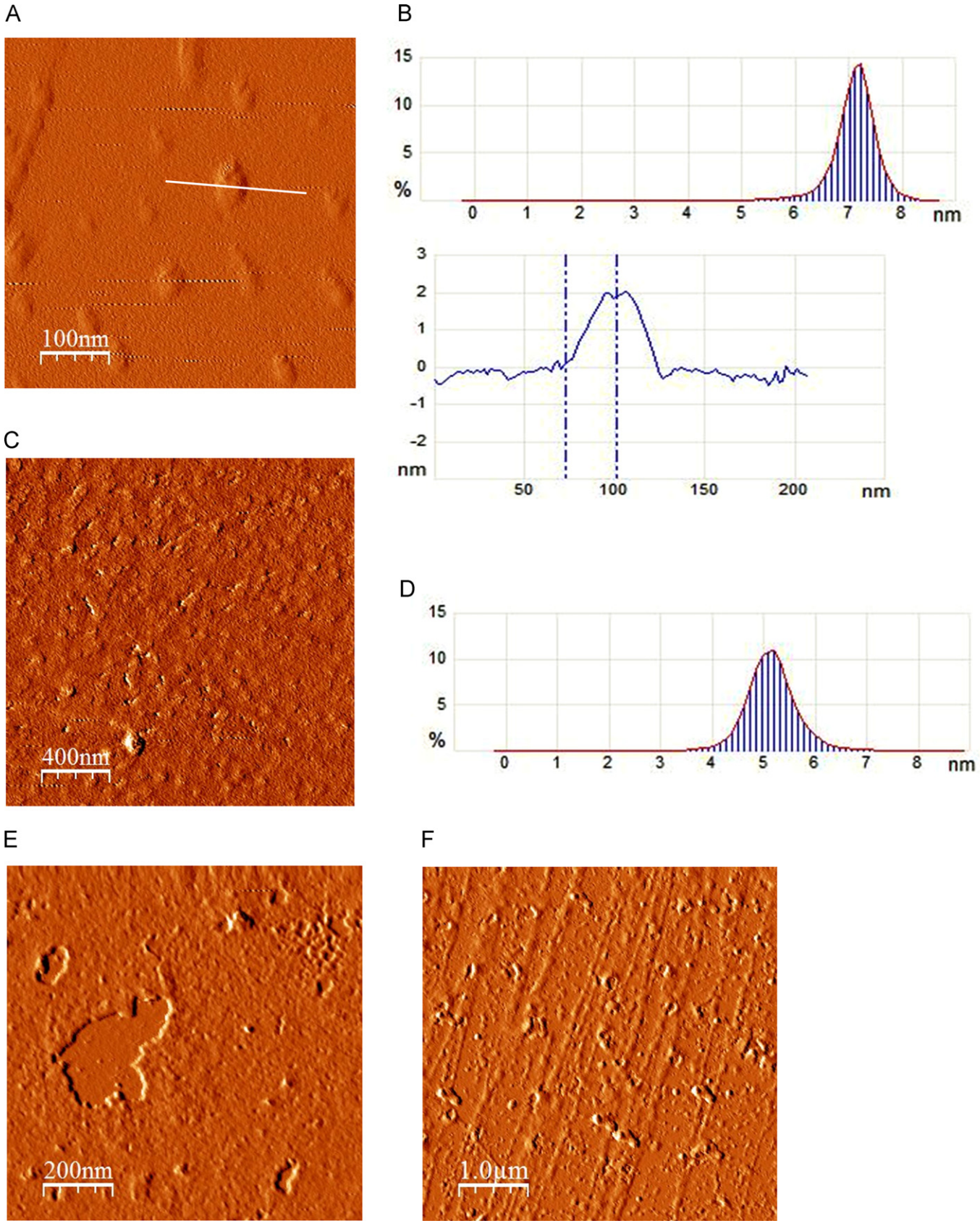

Fig. 2. AFM study of polycarbolxylated thiacalix[4]arene film prior to (A–D) and after the NR binding (E,F). The concentration of macrocyclic receptor was 5(A,E) and 50 (C,F) nM/cm^2. Histograms (B,D) represent the height distribution of nanoparticles within the 2×2 μm^2 area. The cross-section profile (*B*) corresponds to the white line in Fig. 2A.

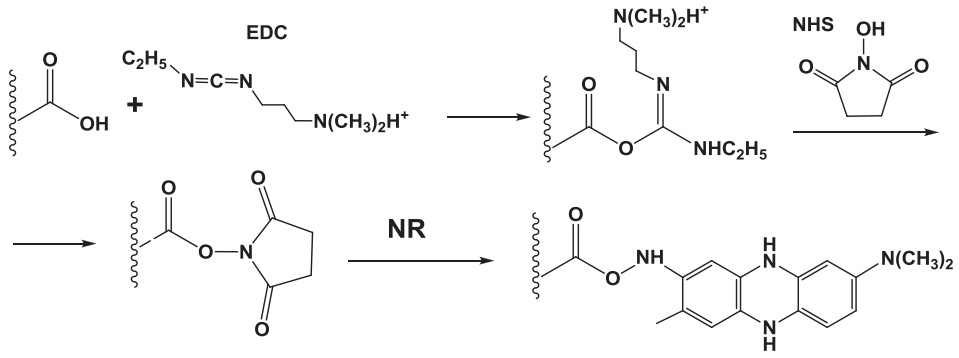

Scheme 2

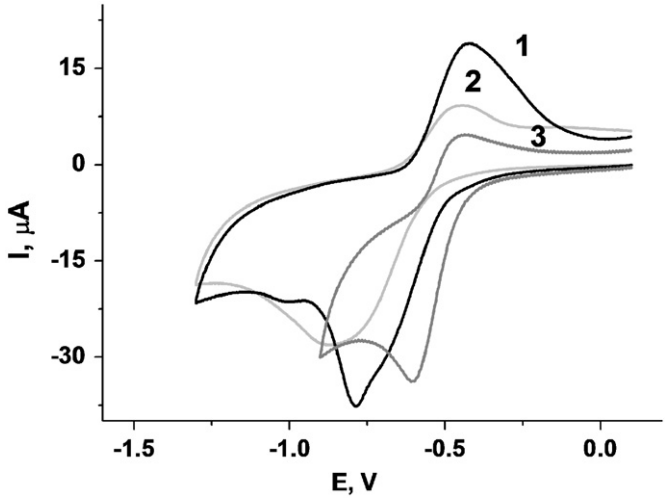

Fig. 3. Cyclic voltammograms recorded on GCE modified with thiacalix[4]arene in configuration *cone* (1) and 1,3-*alternate* (2) and *partial cone* (3) bearing the NR fragments, 0.05 HEPES, pH=7.0, 0.1 V/s.

contained a pair of asymmetrical peaks at $-0.56,\ldots,-0.70$ V related to the NR redox conversion (3) [37]

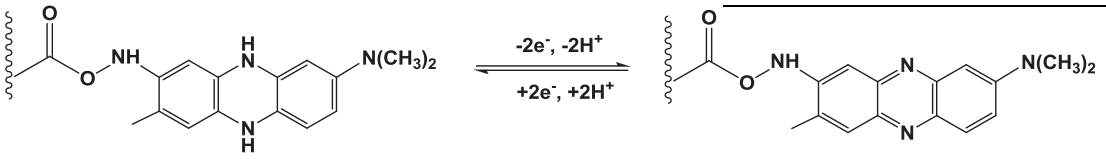

All the experiments were performed in HEPES at pH 7.0. These conditions corresponded to maximal and most reproducible current recorded. The use of TRIS instead of the HEPES buffer solution in the stage of electrochemical measurements decreased the NR peak current by 15–25%. No significant changes in the peak current and its resolution were observed by varying the incubation time at different stages of the carbodiimide binding.

The prevalence of the cathodic peak can be referred to as the electron exchange within the surface layer which controls the distribution of oxidized and reduced NR groups. Indeed, we have found a linear relationship between the cathodic and anodic peak currents and the square root of the scan rate indicating diffusion like processes of electron transfer at the electrode interface. As far as the mediator is covalently bonded to the macrocyclic carrier, this can be due to the hopping mechanism of an electron transfer between neighboring redox centers belonging to the same or different macrocyclic moieties. A similar behavior was reported for the electrodes

Table 1
The calibration equations and analytical characteristics of the thrombin determination with voltammetric aptasensors based on various configurations of polycarboxylated thiacalix[4]arene attached to NR. Mean ± S.D. values were calculated for the results obtained with six aptasensors.

Thiacalix[4]arene configuration	ΔI, μA, $= a + b$ log (Thrombin, nM)			LOD (nM)	Concentration range (nM)
	a	b	R^2		
cone	1.9 ± 0.3	5.0 ± 0.2	0.947	0.8	5–100
paco	1.8 ± 0.3	4.5 ± 0.2	0.958	0.3	5–100
1,3-*alternate*	0.9 ± 0.2	3.2 ± 0.2	0.969	1.0	5–200

covered with non-conductive polymers bearing ferrocene units [38,39]. At a high degree of ferrocene substitution, apparent diffusion limited voltammgrams were obtained with the peaks corresponded to the hopping electron transfer from one ferrocene unit to another.

The effective concentration of mediator forms on the electrode was calculated from Eq. (1) [40]:

$$i_p = (n^2F^2\nu A\Gamma)/(4RT) \quad (1)$$

where i_p is the peak current, n is the number of electrons transferred, A is the area of the electrode, Γ is the surface coverage of redox species and v is the scan rate. For cathodic peak, the surface coverage was found to be 22 ± 3, 12 ± 4 and 17 ± 4 nM/cm^2 for *cone*, *paco* and 1,3-*alternate* configurations, respectively. The nominal surface concentration of thiacalix[4]arene was 60 nM/cm^2 and each molecule of thiacalix[4]arene has eight terminal carboxylic groups, so that there are enough binding sites for the aptamer immobilization. The latter stage decreases the NR signal by about 20% against the thiacalix[4]arene—NR aggregate. This coincides with the mechanism of hopping electron exchange and is related to changes in the flexibility of the substituents linked to the redox centers.

The incubation of the aptasensor in the thrombin solution results in a gradual decrease of the NR current due to binding of the protein in the proximity of redox centers of the surface layer. The appropriate voltammograms for *cone* and *paco* configurations are presented in supplementary materials. The influence of the NR carrier on the sensitivity of the signal toward thrombin is shown in Table 1 for the shift of the reduction peak ΔI, μA, against

thrombin concentration. Since the thiacalix[4]arene configurations displayed different NR peak currents (see Fig. 3), relative values were used for calculation and comparison of the calibration equations. A 100% level corresponds to the reduction peak current observed after the aptamer binding and prior to the contact of an aptasensor with thrombin.

The *paco* and *cone* configurations with most approximated carboxylic units showed higher sensitivity of the signal against 1,3-*alternate* with freely located substituents. The appropriate slope values are differed by 1.5. All the configurations did not vary in the concentration range which covered about two orders of thrombin magnitude, from 1 to 200 nM (the LOD value corresponded to $S/N=3$ ratio). The RSD value of the signal toward thrombin measured with 6 aptasensors did not exceed 3.5% (for six replications at 10 nM thrombin). The aptasensor preserved the main characteristics of the NR redox activity and sensitivity toward thrombin within 2 weeks of continuous operation.

The characteristics of the aptasensor based on *paco* isomer coincide with the previously reported sensitivity data obtained in similar conditions with other composition of the surface layer [33]. Other configurations of the macrocycle showed similar sensitivity with a maximal decay of the initial signal which did not exceed 45% of initial value.

3.3. EIS measurements

EIS is a powerful tool for the investigation of the charge transfer phenomena on the electrode interface. Changes in the charge transfer resistance (R_{et}) and capacitance (C) are interpreted in terms of the changes related to the charge separation or diffusion limitations caused by biorecognition events in the surface layer. The dimensionless index α which determined the sense of constant phase angle element was higher than 0.85 in all the experiments. Thus pure capacitance C can be used for this variance [41].

The Nyquist diagrams contained one semi-circle indicating the charge transfer limitation on the electrode interface (Fig. 4). The resistance slightly decayed while aptamer was bonded to thiacalix[4]arene—NR aggregates. This might be due to shielding the negative charge of the carboxylic groups of the macrocycle.

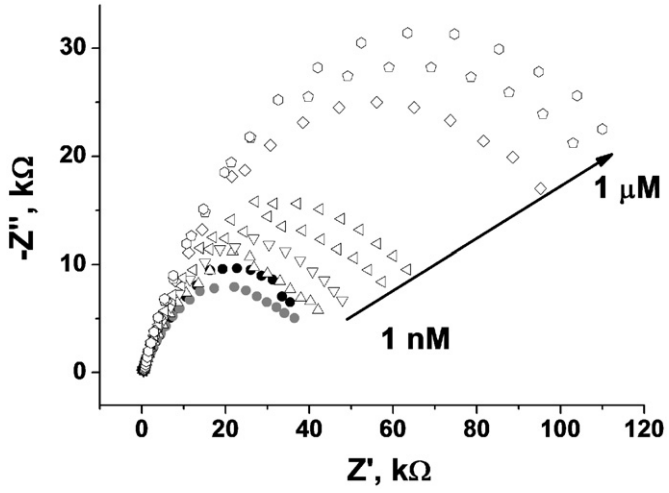

Fig. 4. Nyquist diagrams of impedance spectra obtained at the aptasensor based on 1,3-*alternate* of thiacalix[4]arene with covalently attached NR (gray circles), after aptamer immobilization (black circles) and in the presence of 1, 5, 10, 50, 100, 500 and 100 nM thrombin (open symbols, arrow shows the direction of concentration increase). Measurements in the presence of 0.01 M $K_3[Fe(CN)_6]$ and 0.01 M $K_4[Fe(CN)_6]$ at 0.235 V vs. Ag/AgCl. Frequency range from 0.04 Hz to 100 kHz, amplitude 5 mV.

Table 2
The calibration equations and analytical characteristics of the thrombin determination with impedimetric aptasensors based on various configurations of polycarboxylated thiacalix[4]arene attached to NR. Mean ± S.D. values were calculated for the results obtained with six aptasensors.

Thiacalix[4]arene configuration	ΔR, kΩ$=a+b\times\log$ (Thrombin, nM)			LOD (nM)	Concentration range (nM)
	a	b	R^2		
cone	50 ± 1	12 ± 1	0.929	0.5	5–1000
paco	72 ± 2	11 ± 1	0.924	0.3	5–1000
1,3-*alternate*	45 ± 2	48 ± 3	0.972	0.05	1–1000
	C, μF$=a-b\times\log$ (Thrombin, nM)				
	a	b	R^2		
cone	5.0 ± 0.1	0.5 ± 0.1	0.912	4.0	10–1000
paco	4.3 ± 0.2	0.5 ± 0.1	0.901	8.0	50–1000
1,3-*alternate*	7.6 ± .7	1.2 ± 0.2	0.826	1.0	10–1000

After that the resistance started growing because of the deposition of the thrombin molecules which increased the diffusional hindrance of the redox indicator access to the electrode interface.

The characteristics of the EIS are presented in Table 2. The charge transfer resistance showed maximal sensitivity toward thrombin and changed by more than 400% of the initial value within the concentration range examined. This is due to the combination of both mechanisms of the signal generation, i.e., (i) shielding the positive charge of the mediators which suppresses the electrostatic attraction of negatively charged ferricyanide ions and (ii) diffusion limitation due to the deposition of rather bulky thrombin molecules.

The consideration of the finite thickness of the surface layer with the $R(RC)(RC)$ equivalent circuit showed that the interaction with thrombin insignificantly affects the resistance of the charge transfer on the inner interface (electrode—biorecognition layer) for *cone* and *paco* isomers. Contrary to that, 1,3-*alternate* showed a comparable shift of inner and outer resistance. This coincides well enough with the difference in the voltammetric characteristics of thrombin detection (Table 1). Probably, 1,3-*alternate* forms a less compact surface layer so that the thrombin binding changes the characteristics of the full coverage, whereas other isomers coordinate the analyte predominantly on the surface of the layer. The distribution of the capacitance on both interfaces is about the same and does not differ dramatically from each other.

3.4. Sensitivity and selectivity of thrombin detection

It should be noted that the relative sensitivity of the thiacalix[4]arene configurations of impedimetric and voltammetric measurements differs from each other. Thus, the highest slope of the calibration curve was obtained for 1,3-*alternate* based on R_{et} and C measurements (Table 2) whereas *paco* and *cone* provided almost the same characteristics for both methods. The lowest LOD value among all the techniques used was obtained for 1,3-*alternate* (0.05 nM). In general, the sensitivity of EIS aptasensors was higher than that of voltammetric measurements even though the difference was not so significant. The use of capacitance as an aptasensor response seems less reasonable. Probably, this is due to the diversity of factors affecting the charge distribution and hence the capacitance shift. Besides target aptamer–thrombin interactions, the charge depends on the distribution of reduced and oxidized groups of thiacalix[4]arene—NR aggregates and can be influenced by local pH changes within the surface layer due to redox conversion of the mediator (see Eq. (1)).

Table 3
Comparison of the analytical characteristics of electrochemical aptasensors for thrombin determination.

Sensing layer, measurement mode[a]	LOD	Concentration range	Ref.
Silica nanoparticles with thiolated ferrocene, sandwich two-aptamer binding, DPV	0.06 nM	0.1–5 nM	[5]
Polythionine onto Au modified with Nafion, DC	40 pM	0.12–46 nM	[11]
Self-assembled monolayer with ferrocene label, DPV and EIS	0.5 nM	5–225 nM	[13]
GCE covered with Au nanoparticles, DC	1 nM	10 nM to 10 μM	[19]
GCE, Au labeled aptamer, displacement type assay, DPV	0.66 pM	1.5–45 pM	[21]
Poly(methylene green) with molecular imprints, EIS	0.5 nM	1 nM to 1 μM	[31]
Poly(methylene blue) and poly(methylene green), potentiometry and EIS	–	1 nM to 1 mM	[30]
Au electrode, aptamers with ferrocene labels, sandwich immunoassay, DC	0.14 pM	0.14–56 pM	[42]
Au electrode, sandwich type binding with implementation of Pb nanoparticles, SV	6.2 fM	0.04–0.75 pM	[43]
PAMAM dendrimer with covalently linked aptamer, EIS	0.01 nM	1–50 nM	[44]
Au electrode, CdS quantum dots, sandwich type assay, DPV	0.55 fM	1 fM to 10 pM	[45]
Au nanoparticles onto Au electrode covered with 1,6-hexanedithiol, EIS	0.013 nM	0.1–30 nM	[46]
Au electrode with self-assembled monolayer, aptamer labeled with Fe_3O_4 nanoparticles, DPV	0.1 nM	1–75 nM	[47]

[a] DPV:differential pulse voltammetry; DC:direct current voltammetry; SV:stripping voltammetry.

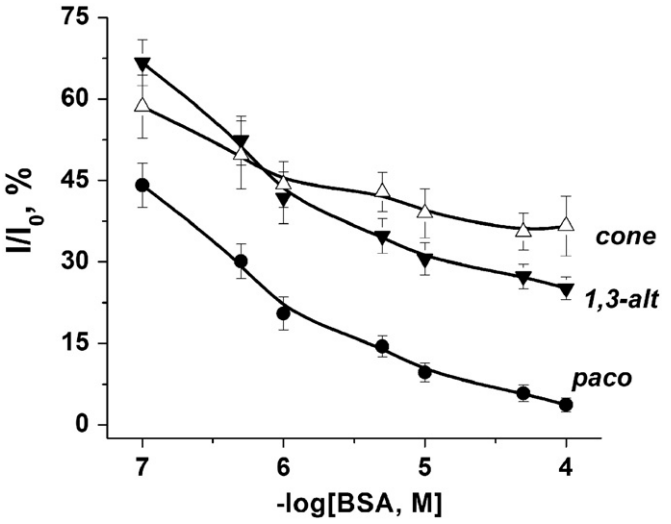

Fig. 5. Relative changes in the NR reduction peak current recorded on aptasensors based on various carboxylated thiacalix[4]arenes as a function of the BSA concentration. HEPES buffer solution, pH=7.0.

The aptasensor developed showed the sensitivity toward thrombin comparable with that of many other detection systems reported so far (Table 3). Most sensitive biosensors with the LOD below 0.1 nM employ multi-stage accumulation of the target analyte based on immunoassay approaches, magnetic separation or hybridization of differently labeled aptasensors. In addition, stripping voltammetry with the anodic dissolution of metal nanoparticles used as aptamer or anti-thrombin antibody labels showed excellent results.

Being very sensitive, such aptasensors are time and labor consuming and require specific subsidiary reagents. Contrary to that, the biosensor developed made it possible to perform thrombin determination in one step with a minimal additional treatment of the samples.

The selectivity of the response toward thrombin was examined using BSA solution in the same conditions as it has been previously specified for thrombin detection. As in the case of thrombin, the reduction current decayed (Fig. 5), but in the concentration range far from that of target analyte. Moreover, measurements of the signal in binary mixtures of thrombin and BSA showed that the influence of the latter was even lower than in the model solution (results are not shown). Thus, the presence of 10 μM BSA did not alter the signal of 1 nM thrombin for all the thiacalix[4]arene configurations used. It should be, however, noted, that physiological concentrations of albumins in blood are around 0.6 mM [48]. As it is seen from Fig. 5, at this concentration of BSA the changes of NR reduction peak are rather high for aptasensor based on calixarenes in *paco* configuration, but less expressed for that based in *cone* configuration. Considering rather high sensitivity of the aptasensors it is likely that they can be used in at least 10 times in diluted real samples, e.g. blood plasma or serum. This may eliminate the effect of albumins. Further effort is, however, required for sensor validation. These experiments are in progress.

4. Conclusion

The use of a new kind of mediator, i.e., NR attached to the macrocyclic carrier, offered new opportunities for DNA-sensor and aptasensor development. In addition to the preliminary report [33] which could be considered as a "proof of concept", the following new investigations have been performed:

(1) The optimal density of the surface layer coverage was selected based on the AFM data displaying full coverage of the support and regular structure of the surface changing with the NR binding.
(2) The EIS investigation of the charge transfer on the electrode interface confirmed two possible mechanisms for the signal generation, i.e., the spatial limitations of the electron exchange between reduced and oxidized NR fragments within the surface layer and increased diffusional limitation of the charge carrier transfer (ferricyaninde ion) due to thrombin binding.
(3) The influence of the configuration of the macrocyclic carrier (*cone*, *paco* and 1,3-*alternate*) on the performance of the aptasensor was discovered and explained by the different accessibility of the NR bearing substituents and aptamer in the reactions of electron exchange and analyte binding, respectively.

Even though the assembly of the biorecognition layer was simplified by removing internal layer of poly-NR as compared to that described in the preliminary report [33], the reproducibility of the response was quite comparable with that observed for other aptasensors based on conventional mediators. The increased loading of the macrocyclic receptor providing full and dense coverage of the GCE surface can be a possible reason for the low LOD (down to 0.05 nM). The analytical characteristics of the thrombin determination are sensitive enough for its direct reagent free determination in blood serum within 20 min. No special sample treatment is required.

The immobilization scheme and approaches to the surface layer optimization based on the combination of EIS and AMF data can be easily applied to other similar mediators and biorecognition systems, e.g., the detection of the hybridization events by DNA sensors or sandwich type and competitive immunosensors. This makes it possible to simplify the biosensor development and the application of generic signal measurement schemes with pre-determined characteristics of the signal.

Acknowledgments

The financial support by the Russian Foundation for Basic Research (Grant 11-03-00381 to G.E. and A.P.), Ministry of Science and Education of Russian Federation (Grant 16.740.11.0496 to G.E.) and the National Scholarship Program of Slovak Republic (V.K.) is greatly acknowledged. T.H. is grateful to Slovak Research and Development Agency (Contract nos. APVV-0410-10 and LPP-0341-09) and VEGA (Project no. 1/0785/12) for financial support. The authors thank Nanotechnology Research Center of Kazan National Research Technological University (KNITU) for possibility of AFM study.

Appendix A. Supporting information

Supplementary data associated with this article can be found in the online version at http://dx.doi.org/10.1016/j.talanta.2012.07.007.

References

[1] R. Mukhopadhyay, Anal. Chem. 77 (2005) 115A–118A.
[2] M. Mascini, Anal. Bioanal. Chem. 390 (2008) 987–988.
[3] S. Song, L. Wang, J. Li, J. Zhao, C. Fan, Trends Anal. Chem. 27 (2008) 108–117.
[4] Y.L. Zhang, P.-F. Pang, J.-H. Jiang, G.L. Shen, R.Q. Yu, Electroanalysis 21 (2009) 1327–1333.
[5] Y. Wang, X. He, K. Wang, X. Ni, J. Su, Z. Chen, Biosens. Bioelectron. 26 (2011) 3536–3541.
[6] P. Tong, L. Zhang, J.J. Xu, H.Y. Chen, Biosens. Bioelectron. 29 (2011) 97–101.
[7] G.S. Bang, S. Cho, B.G. Kim, Biosens. Bioelectron. 21 (2005) 863–870.
[8] A. Porfirieva, G. Evtugyn, T. Hianik, Electroanalysis 19 (2007) 1915–1920.
[9] G. Evtugyn, A. Porfireva, M. Ryabova, T. Hianik, Electroanalysis 20 (2008) 2310–2316.
[10] H. Qin, J. Liu, C. Chen, J.H. Wang, E. Wang, Anal. Chim. Acta 712 (2012) 127–131.
[11] Y. Yuan, R. Yuan, Y. Chai, Y. Zhuo, Z. Liu, L. Mao, S. Guan, X. Qian, Anal. Chim. Acta 668 (2010) 171–176.
[12] A.-E. Radi, C.K. O'Sullivan, Chem. Commun. (2006) 3432–3434.
[13] A.-E. Radi, J.L.A. Sánchez, E. Baldrich, C.K. O'Sullivan, J. Am. Chem. Soc. 128 (2006) 117–124.
[14] G. Cheng, B. Shen, F. Zhang, J. Wu, Y. Xu, P. He, Y. Fang, Biosens. Bioelectron. 25 (2010) 2265–2269.
[15] B. Li, Y. Wang, H. Wei, S. Dong, Biosens. Bioelectron. 23 (2008) 965–970.
[16] Y. Du, B. Li, F. Wang, S. Dong, Biosens. Bioelectron. 24 (2009) 1979–1983.
[17] Y. Chai, D. Tian, J. Gu, H. Cui, Analyst 136 (2011) 3244–3251.
[18] S. Guo, Y. Du, X. Yang, S. Dong, E. Wang, Anal. Chem. 83 (2011) 8035–8040.
[19] E. Suprun, V. Shumyantseva, T. Bulko, S. Rachmetova, S. Rad'ko, N. Bodoev, A. Archakov, Biosens. Bioelectron. 24 (2008) 831–836.
[20] P. Chandra, H.B. Noh, M.-S. Won, Y.B. Shim, Biosens. Bioelectron. 26 (2011) 4442–4449.
[21] J.J. Zheng, G.-F. Cheng, P.-G. He, Y.-Z. Fang, Talanta 80 (2010) 1868–1872.
[22] B.K. Das, C. Tlili, S. Badhulika, L.N. Cella, W. Chen, A. Mulchandani, Chem. Commun. 47 (2011) 3793–3795.
[23] P. Blondeau, F.X. Rius-Ruiz, A. Düzgün, J. Riu, F.X. Rius, Mater. Sci. Eng. C 31 (2011) 1363–1368.
[24] C.A. Holland, A.T. Henry, H.C. Whinna, F.C. Church, FEBS Lett. 484 (2000) 87–91.
[25] L.C. Bock, L.C. Griffin, J.A. Latham, E.H. Vermaas, J.J. Toole, Nature 355 (1992) 564–566.
[26] D.M. Tasset, M.F. Kubik, W. Steiner, J. Mol. Biol. 272 (1997) 688–698.
[27] R.F. Macaya, P. Schulte, F.W. Smith, J.A. Roe, J. Feigon, Proc. Natl. Acad. Sci. USA 90 (1993) 3745.
[28] J. Bichler, J.A. Heit, W.G. Owen, Thromb. Res. 84 (1996) 289.
[29] J. Müller, T. Becher, J. Braunstein, P. Berdel, S. Gravius, F. Rohrbach, J. Oldenburg, G. Mayer, B. Pötzsch, Angew. Chem. Int. Ed. 50 (2011) 6075–6078.
[30] G.A. Evtugyn, A.V. Porfireva, T. Hianik, M.S. Cheburova, H.C. Budnikov, Electroanalysis 20 (2008) 1300–1308.
[31] G. Evtugyn, A. Porfireva, A. Ivanov, O. Konovalova, T. Hianik, Electroanalysis 21 (2009) 1272–1277.
[32] A.V. Porfireva, G.A. Evtugyn, A.N. Ivanov, T. Hianik, Electroanalysis 22 (2010) 2187–2195.
[33] G. Evtugyn, V. Kostyleva, R. Sitdikov, A. Porfireva, M. Savelieva, I. Stoikov, I. Antipin, T. Hianik, Electroanalysis 24 (2012) 91–100.
[34] G.A. Evtugyn, R.R. Younusov, A.N. Ivanov, R.R. Sitdikov, A.V. Galuchin, H.C. Budnikov, I.I. Stoikov, I.S. Antipin, Electroanalysis 24 (2012) 554–562.
[35] C. Ocaña, M. Pacios, M. del Valle, Sensors 12 (2012) 3037–3048.
[36] M. Strobel, K. Kita-Tokarczyk, A. Taubert, C. Vebert, P.A. Heiney, M. Chami, W. Meier, Adv. Funct. Mater. 16 (2006) 252–259.
[37] R. Pauliukaite, C.M.A. Brett, Electroanalysis 20 (2008) 1275–1285.
[38] A.L. Crumbliss, D. Cooke, J. Castillo, P. Wisian-Neilson, Inorg. Chem. 32 (1993) 6088–6094.
[39] M. Watanabe, H. Nagasaka, N. Ogata, J. Phys. Chem. 99 (1995) 12294–12300.
[40] A.J. Bard, L.R. Faulkner, Electrochemical Methods: Fundamentals and Applications, Willey, New York, 1982.
[41] J.-B. Jorcin, M.E. Orazem, N. Pébère, B. Tribollet, Electrochim. Acta 51 (2006) 1473–1479.
[42] M.A. Rahman, J.I. Son, M.-S. Won, Y.-B. Shim, Anal. Chem. 81 (2009) 6604–6611.
[43] Y. Xiao, P.D. Piorek, K.W. Plaxco, A.J. Heeger, J. Am. Chem. Soc. 127 (2005) 17990–17991.
[44] Z. Zhang, W. Yang, J. Wang, C. Yang, F. Yang, X. Yang, Talanta 78 (2009) 1240–1245.
[45] C. Ding, Y. Ge, J.-M. Lin, Biosens. Bioelectron. 25 (2010) 1290–1294.
[46] L.D. Li, H.T. Zhao, Z.-B. Chen, X.J. Mu, L. Guo, Sensors Actuators B 157 (2011) 189–194.
[47] S. Zhang, G. Zhou, X. Xu, L. Cao, G. Liang, H. Chen, B. Liu, J. Kong, Electrochem. Commun. 13 (2011) 928–931.
[48] A. Barzegar, A.A. Moosavi-Movahedi, N. Sattarahmady, M.A. Hosseinpour-Faizi, M. Aminbakhsh, F. Ahmad, A.A. Saboury, M.R. Ganjali, P. Norouzi, Protein Peptide Lett. 14 (2007) 13–18.